PHYSICAL REVIEW B VOLUME 20, NUMBER 11 1 DECEMBER 1979

Defects in the two-dimensional electron solid and implications for melting

Daniel S. Fisher and B. I. Halperin
Bell Laboratories Murray Hill, New Jersey 07974
and Harvard University, Cambridge, Massachusetts 02138

R. Morf
Harvard University, Cambridge, Massachusetts 02138
(Received 27 July 1979)

We have calculated the energies of formation for various defects in a two-dimensional electron lattice. Included are vacancies and interstitials, dislocation pairs, and grain boundaries. From the results, we have extracted the dislocation core energy, and an approximate formula for the grain boundary energy as a function of angle. We discuss some possible implications for melting, and for dynamic processes such as electron diffusion and dislocation migration.

I. INTRODUCTION

There has been considerable interest recently in two-dimensional classical systems of electrons, and in particular in the possible formation of a two-dimensional electron crystal.[1] Recent experiments by Grimes and Adams[2] on electrons trapped at the surface of liquid helium found several resonances in the rf absorption of the system which appeared suddenly as the system was cooled through a transition temperature T_c which lies in the range of a few tenths of a kelvin for electron densities (n_s) of a few times 10^8 electrons/cm^2. The experiment has been analyzed by Fisher, Halperin, and Platzman[3] who show that excellent agreement with the data can be obtained from a theory which assumes the existence of a triangular electron lattice at temperatures below T_c.

In order to understand the electron system in more detail, it is important to investigate properties of the classical two-dimensional electron crystal. Several authors[4,5] have calculated ground-state energies and phonon spectra for various electron lattices at zero temperature. However, in order to understand finite-temperature static and dynamic properties, it is also necessary to investigate deviations from a perfect crystal, i.e., defects. Localized defects (i.e., vacancies, interstitials, divacancies, etc.) will be present in finite concentrations at any nonzero temperature and will be important for dynamical processes in the crystal. Extended defects, (dislocations, grain boundaries, etc.) while not present individually at low temperatures due to their large energies, may nevertheless play important roles in the melting of the crystal.[6,7]

In the present paper, we present the results of numerical calculations of the energies of various defects in the two-dimensional electron crystal. (A system of 780 electrons with periodic boundary conditions has been used for the numerical computations.) We briefly discuss the important interactions between these defects and possible implications of our calculations on theories of two-dimensional melting and dynamical processes in the electron solid.

The remainder of this section is devoted to discussion of the ground state and useful conventions for defining defect energies. In Sec. II below, we compare numerical and elasticity theory calculations for the energy of a vacancy and also exhibit numerical results for interstitials, divacancies, and other localized defects. In Sec. III, we present analytical and numerical results on dislocations, the defects important in the Kosterlitz-Thouless-Halperin-Nelson-Young theory of two-dimensional melting.[6-8] Section IV deals with grain boundaries and their analysis as arrays of dislocations and Sec. V discusses melting and dynamical processes. Discussion of the numerical calculation is contained in the Appendix.

A. Conventions for energies

We now consider the ground state of the electron system. To sensibly define energies in a Coulomb system, a background of positive charge is needed. (The background is provided by image charges in a distant metal plate in the case of electrons on helium.) If we include this positive background, then the energy of a Bravais lattice of N electrons (and their associated uniform positive background) is

$$E = -\tfrac{1}{2} N E_B \ , \tag{1.1}$$

where E_B, the energy required to remove one electron and its positive background, is given by

$$E_B = e^2 \sum_{\vec{R}\neq 0} \frac{1}{|\vec{R}|} - \frac{e^2}{A_c} \sum_{\vec{R}} \int_{C_{\vec{R}}} \frac{d^2 r}{|\vec{r}|} \ , \tag{1.2}$$

where $\{\vec{R}\}$ are lattice vectors and $C_{\vec{R}}$ is the unit cell

centered at $\vec{R}$ with area A_c.

Both the sums in Eq. (1.2) are divergent at large $\vec{R}$ but their difference is well defined and can be calculated numerically by Ewald's method for Madelung sums. The energy E_B has been calculated for various lattices and it is found that for a given density, the triangular lattice has the lowest energy of all the Bravais lattices with one electron per unit cell.[4] The result is

$$E_B = 3.921\epsilon_0 \equiv \epsilon_B A_c^{-1/2} \ , \tag{1.3}$$

where

$$\epsilon_0 = e^2 A_c^{-1/2} \tag{1.4}$$

is the natural unit for energy which will be used throughout this paper. For a perfect lattice

$$n_s = \frac{1}{A_c} \tag{1.5}$$

and for the triangular case,

$$A_c = \tfrac{1}{2}\sqrt{3}a_0^2 \ , \tag{1.6}$$

where a_0 is the lattice spacing.

The energy of a square lattice is[4]

$$E_B^{\square} = 3.900\epsilon_0 \ , \tag{1.7}$$

rather close to that of the triangular lattice, but at zero temperature it has an unstable shear mode. However, one cannot rule out the possibility that in some range of temperatures the square lattice (or some other) is favored over the triangular lattice by entropy considerations. We will not discuss this possibility here and will content ourselves with the observation that the experiments of Grimes and Adams[2,3] are very consistent with the assumption of a triangular lattice at all temperatures below melting, and restrict ourselves to this case throughout the paper.

We now turn to the question of definition of defect energies. Let us consider a system with N electrons (and their compensating positive background) in an area, A, with density

$$n_s = \frac{N}{A} \ . \tag{1.8}$$

We rearrange the N electrons to form a lattice with a defect and define the energy of the defect as the limit as $A \to \infty$ (with n_s constant) of the difference between the energy of the rearranged lattice and a perfect crystal.

For definiteness let us consider a single vacancy. In this case the rearranged lattice will have one more cell than the original lattice. If we neglect the distortion produced by the missing electron, the area of the new unit cell is given by

$$A_c' = \frac{A}{N+1} \ . \tag{1.9}$$

We now let the lattice relax to its new equilibrium. The limit as $N \to \infty$ of the energy of this rearranged lattice is well defined as long as the density and the corresponding positive background remain constant.

In the computer calculations, we have not an infinite system but a system with a large but finite block of particles with periodic boundary conditions. For comparison with the computer results, we must therefore calculate not the energy of a single defect in an infinite system, but the energy per block of a periodic array of defects in an infinite system. Discussion of how this is done is included under each individual type of defect considered. After correcting for these "image" defects we can extract the desired energy of a single defect.

II. VACANCIES, INTERSTITIALS, AND OTHER LOCALIZED DEFECTS

In this section we first calculate the energy of a single vacancy in a triangular lattice by a variational method with several approximations and compare this to computer calculations. Second, we discuss similar calculations for other simple defects and finally present computer results for the energies of interstitials and other localized defects.

A. Definition of vacancy energy

It is convenient to calculate energies of vacancies, etc., at constant *lattice spacing* rather than the desired energy at constant density (as discussed in the Introduction) and then correct for the difference.

Let us consider again for definiteness, the case of a vacancy in a system of N electrons in area A. If the computed energy of this system is E, then the defect energy is

$$E_D = E + \tfrac{1}{2}N\epsilon_B(N/A)^{1/2} \ , \tag{2.1}$$

where the second term is just the negative of the energy of the perfect crystal with the same number of particles N. The energy of a perfect crystal with the same *lattice spacing* is

$$-\tfrac{1}{2}(N+1)\epsilon_B[(N+1)/A]^{1/2} \ , \tag{2.2}$$

and hence the energy at constant *lattice* spacing is

$$E_D^{(2)} = E + \tfrac{1}{2}(N+1)\epsilon_B[(N+1)/A]^{1/2} \ . \tag{2.3}$$

For large N, we then find that

$$E_D = E_D^{(2)} - \tfrac{3}{4}\epsilon_B n_s^{1/2} \ . \tag{2.4}$$

This can be generalized for defects which differ from a perfect lattice by addition of N_D (or subtraction of $-N_D$) electrons to

$$E_D = E_D^{(2)} + \tfrac{3}{4}N_D\epsilon_B n_s^{1/2} \ , \tag{2.5}$$

where $E_D^{(2)}$ is the energy calculated at constant lattice spacing. In this section we will calculate energies at constant lattice spacing, and then use Eq. (2.5) to correct the result.

The energy of a vacancy is given by

$$E_V = E_B + E_{VR} - \tfrac{3}{4}E_B \ , \tag{2.6}$$

where the first term E_B (as defined above) is the energy required to remove one electron and its positive background without allowing the lattice to relax, the second is the relaxational energy, and the third is the correction given by Eq. (2.4).

B. Elasticity theory

Before proceeding with our calculation of the vacancy relaxational energy, E_{VR}, it is useful to digress and review elasticity theory.

If we have an electron crystal with the electrons at each site displaced slightly from equilibrium, then the additional potential energy is

$$\Delta E = \tfrac{1}{2}e^2 \sum_{l \neq l'} \frac{1}{|\vec{x}(l) + \vec{u}(l) - \vec{x}(l') - \vec{u}(l')|} - \frac{1}{|\vec{x}(l) - \vec{x}(l')|} \ , \tag{2.7}$$

where the sums run over lattice sites l, and $u(l)$ is the deviation of the lth site from its equilibrium position.

If the displacements, $\vec{u}$, are small with respect to the lattice spacing, a_0, we can expand the energy in powers of $\vec{u}$ and obtain

$$\Delta E = \tfrac{1}{2}e^2 \sum_{ll'} \Pi_{\alpha\beta}(l,l') u_\alpha(l) u_\beta(l') \ , \tag{2.8}$$

where

$$\Pi_{\alpha\beta}(l,l') = \frac{-3[x_\alpha(l) - x_\alpha(l')][x_\beta(l) - x_\beta(l')]}{|\vec{x}(l) - \vec{x}(l')|^5} + \frac{\delta_{\alpha\beta}}{|\vec{x}(l) - \vec{x}(l')|^3} \ , \quad \text{for } l \neq l'$$

and

$$\Pi_{\alpha\beta}(l,l) = \sum_{l' \neq l} \Pi_{\alpha\beta}(l,l') \ . \tag{2.9}$$

We can Fourier transform Eq. (2.4) to obtain

$$\Delta E = \frac{1}{2}\frac{e^2}{A_c^2} \int_{\vec{q}} u_\alpha(\vec{q}) u_\beta(-\vec{q}) \Pi_{\alpha\beta}(\vec{q}) \ , \tag{2.10}$$

(sums over repeated indices implied) where

$$u_\alpha(\vec{q}) = A_c \sum_l u_\alpha(l)\, e^{-i\vec{q}\cdot\vec{x}(l)} \ ,$$
$$\Pi_{\alpha\beta}(q) = A_c \sum_l \Pi_{\alpha\beta}(l,0)\, e^{-i\vec{q}\cdot\vec{x}(l)} \ , \tag{2.11}$$

and

$$\int_{\vec{q}} \equiv \left(\frac{1}{2\pi}\right)^2 \int d^2q \ .$$

The phonon frequencies $\omega_i(\vec{q})$ of a perfect electron crystal are given by $\omega_i^2(\vec{q}) = (e^2 n_s/m)\lambda_i$ where λ_i are the eigenvalues of the dynamical matrix $\Pi_{\alpha\beta}(\vec{q})$. For small q, $\Pi_{\alpha\beta}(\vec{q})$ is isotropic because of hexagonal symmetry, and we find[4]

$$\Pi_{\alpha\beta}(\vec{q}) = \frac{2\pi q^\alpha q^\beta}{|q|} + A_c^{1/2}\eta(\delta_{\alpha\beta}q^2 - 6q_\alpha q_\beta) + O(q^4) \ , \tag{2.12}$$

where η is a constant

$$\eta \simeq 0.245\,065 \ . \tag{2.13}$$

The longitudinal phonon branch has the dispersion relation

$$\omega_l^2(q) = \omega_p^2 - \frac{5\eta q^2 e^2}{A_c^{1/2} m} + O(q^4) \ , \tag{2.14}$$

where ω_p is the two-dimensional plasma frequency

$$\omega_p^2(q) = 2\pi \frac{n_s e^2 q}{m} \ . \tag{2.15}$$

(Note the anomalous $\omega \sim \sqrt{q}$ behavior of this plasmalike mode.) The transverse phonon frequency obeys

$$\omega_t^2(q) = \frac{\eta q^2 e^2}{m A_c^{1/2}} \ . \tag{2.16}$$

We wish to compare these phonon frequencies with those for a triangular crystal with short-range forces obtained from continuum elastic theory.

If $\vec{u}(l)$ varies slowly with $\vec{x}(l)$ we can replace the discrete set $\vec{u}(l)$ by a continuous $\vec{u}(\vec{r})$, and the strain energy is given from continuum elastic theory by

$$\mathcal{H} = \int d^2r \left(\mu u_{\alpha\beta}u_{\alpha\beta} + \tfrac{1}{2}\lambda u_{\alpha\alpha}u_{\beta\beta}\right) \ , \tag{2.17}$$

where $u_{\alpha\beta}$ is the strain tensor

$$u_{\alpha\beta} = \frac{1}{2}\left(\frac{\partial u_\beta}{\partial r_\alpha} + \frac{\partial u_\alpha}{\partial r_\beta}\right) \tag{2.18}$$

and μ and λ are the Lamé coefficients. Here we have made use of the hexagonal summetry: there are only two independent elastic coefficients, and the triangular crystal behaves like an isotropic medium. The matrix Π is then (for small q)

$$\Pi_{\alpha\beta}(q) \propto (\mu + \lambda) q_\alpha q_\beta + \mu q^2 \delta_{\alpha\beta} \ , \tag{2.19}$$

and the phonon frequencies are

$$\omega_t^2(q) = \frac{\mu A_c}{m} q^2$$

and

$$\omega_l^2(q) = (2\mu + \lambda)\frac{A_c}{m}q^2 \ . \tag{2.20}$$

We can thus obtain the elastic moduli for the electron crystal by comparison of Eqs. (2.15), (2.16), and (2.20).

From the transverse frequency we find

$$\mu = \eta\frac{e^2}{(A_c)^{3/2}} \ , \tag{2.21}$$

but for the longitudinal frequencies we run into trouble. The appearance of a longitudinal sound velocity in the electron crystal which diverges as $q \to 0$ is equivalent to the observation that the Wigner crystal is incompressible. It is thus natural to choose an effective λ which is infinite. In the experiments with electrons on helium, due to the image charge screening at long distances (as mentioned in the Introduction), λ assumes a finite value given by

$$\lambda \simeq 4\pi n_s^2 e^2 d \ , \tag{2.22}$$

where d is the depth of the helium film. However, this is extremely large ($\lambda/\mu \gtrsim 10^4$), and for the sections of this paper where continuum elasticity theory is used, we will set

$$\lambda = \infty \ . \tag{2.23}$$

C. Variational calculation of vacancy energy

With the connection with elasticity theory clear, we now proceed with the calculation of the vacancy relaxational energy, using the assumption that the deviations from the perfect lattice sites $\{\vec{u}(l)\}$ are small and reasonably slowly varying.

To second order in $\vec{u}(l)$, the relaxational energy for a vacancy at the origin can be obtained by minimization with respect to $\{\vec{u}(l)\}$ of

$$\begin{aligned} E_{\rm VR}(\{\vec{u}(l)\}) = &\tfrac{1}{2}e^2\sum_{l,l'}\Pi_{\alpha\beta}(l,l')u_\alpha(l)u_\beta(l') \\ &- e^2\sum_{l\neq 0}V_1^\alpha(l)u_\alpha(l) \\ &- e^2\sum_{l\neq 0}V_2^{\alpha\beta}(l)u_\alpha(l)u_\beta(l) \end{aligned} \tag{2.24}$$

where

$$V_1^\alpha(l) = \frac{x_\alpha(l)}{|\vec{x}(l)|^3} \ , \tag{2.25}$$

$$V_2^{\alpha\beta}(l) = -\left(\frac{3x_\alpha(l)x_\beta(l) - \delta_{\alpha\beta}\vec{x}^2(l)}{|x(l)|^5}\right) \ ,$$

and $\Pi_{\alpha\beta}(l,l')$ is given by Eq. (2.9). We Fourier transform Eq. (2.25) to obtain

$$\begin{aligned} E_{\rm VR} = &\frac{1}{2}\frac{e^2}{A_c^2}\int_{\vec{q}}u_\alpha(\vec{q})u_\beta(\vec{q})\Pi_{\alpha\beta}(\vec{q}) \\ &- \frac{e^2}{A_c}\int_{\vec{q}}V_1^\alpha(\vec{q})u_\alpha(-\vec{q}) \\ &- \frac{e^2}{2A_c}\int_{\vec{q}}\int_{\vec{r}}V_2^{\alpha\beta}(\vec{q}-\vec{k})u^\alpha(\vec{k})u^\beta(-\vec{q}) \ , \end{aligned} \tag{2.26}$$

where we can easily obtain $V_1^\alpha(\vec{q})$ and $V_2^{\alpha\beta}(\vec{q})$ from $\Pi_{\alpha\beta}(\vec{q})$ by noting that

$$V_2^{\alpha\beta}(\vec{q}) = \tfrac{1}{2}V_2^{\gamma\gamma}(0)\delta_{\alpha\beta} + \Pi_{\alpha\beta}(\vec{q}) \ , \tag{2.27}$$

where $V_2^{\gamma\gamma}(0)$ is a constant which will drop out of Eq. (2.26) for the energy by symmetry under $\vec{q} \to -\vec{q}$, and

$$\begin{aligned} V_1^\alpha(\vec{q}) &= -i\frac{\partial}{\partial q_\alpha}\Pi_{\gamma\gamma}(\vec{q}) \\ &= -\frac{i2\pi q_\alpha}{|q|} + iq_\alpha 8A_c^{1/2}\eta + O(q^3) \ . \end{aligned} \tag{2.28}$$

In order to minimize the energy given by Eq. (2.26) it is necessary to know $\Pi_{\alpha\beta}$ for all q. Bonsall and Maradudin have calculated the phonon spectra for all q, and even away from $q = 0$, it is approximated reasonably well by a $\Pi_{\alpha\beta}$ of the form Eq. (2.12). We thus, for simplicity use Eq. (2.12) for *all* q, hoping that integrating over angles in Eq. (2.26) will cancel most of our errors. [We have found, in any case, that adding terms of order q^4 to Eq. (2.12) does not affect the variational energy appreciably.] In addition we approximate the hexagonal Brillouin zone by a circle of equal area with radius

$$k_D = \frac{4\pi}{A_c^{1/2}} \ . \tag{2.29}$$

With these approximations it is straightforward to do a variational estimate of $E_{\rm VR}$. By our assumed symmetry, $u^\alpha(\vec{q})$ must have the form

$$u_\alpha(\vec{q}) = A_c\frac{q_\alpha}{|q|^2}F(|q|) \ , \tag{2.30}$$

and we try

$$F(q) = f(1 + c|q| + d|q|^2) \ , \tag{2.31}$$

with f, c, and d variational parameters.

Before proceeding with the variational calculation it is instructive to discuss the motivation for choosing this form for $\vec{u}(\vec{q})$.

Because of the long-range Coulomb force between the electrons, we expect that at long distances $\vec{u}(l)$ will be determined by enforcing charge neutrality within any circle about the origin. This yields,

$$u_\alpha(l) \sim -\frac{A_c}{2\pi}\frac{x_\alpha(l)}{|x(l)|^2} \ . \tag{2.32}$$

In Fourier transform, for $q \to 0$, this implies

$$u_\alpha(\vec{q}) = +iA_c \frac{q_\alpha}{|q|^2} \quad . \tag{2.33}$$

In addition by expanding the variational equation for $\vec{u}(q)$ in powers of q one can show that (even including higher powers of $\vec{u}$) $\vec{u}$ is given by Eq. (2.33) plus corrections of order unity (e.g., $q_\alpha/|q|$).

The variational calculation is straightforward and we find that the minimum energy is

$$E_{\rm VR} = -0.59\epsilon_0 \tag{2.34}$$

and

$$f = 0.99 \ , \quad c = -0.26A_c^{1/2} \text{ and } d = 0.009A_c \ . \tag{2.35}$$

This yields a $\vec{u}(\vec{q})$ which is almost independent of $|\vec{q}|$ near the zone edge as is expected by periodicity, and again, as expected f is nearly one.

In order to compare this result for a vacancy in an infinite system with the computer calculations for periodic boundary conditions, we assume that the interactions between vacancies in the periodic array are negligible and hence that we can directly compare the computer results with the above calculation. This assumption is discussed at the end of this section.

From computer calculations we find that

$$E_{\rm VR} = -0.73\epsilon_0 \tag{2.36}$$

and hence a 20% discrepancy between the simple-minded calculation and the computer result. This difference is presumably attributable to nonlinearities and errors caused by the assumption of circular symmetry and approximation of the Brillouin zone by a circle. In this vein, we should note that the maximum calculated displacement u is of the order of $0.12a_0$ and hence our assumptions of small distortions are reasonable. This compares with a maximum displacement of $0.15a_0$ from the computer calculations. The total vacancy energy

$$E_V = \tfrac{1}{4}E_B + E_{\rm VR} \tag{2.37}$$

is given less accurately by the variational calculation since it is the difference of two large energies. The numerical result for the total vacancy energy is

$$E_V = 0.24\epsilon_0 \ . \tag{2.38}$$

A system containing a vacancy is shown in Fig. 1.

D. Other localized defects

It is possible in principle to calculate energies of interstitials and other simple local defects by a similar procedure to that described above for the vacancy. However, while for the vacancy, V_1^α and $V_2^{\alpha\beta}$ are obtainable from the phonon spectrum, this will not generally be the case and the V_1 and V_2 for interstitials must be calculated at small q by evaluating many Ewald sums. In addition, while a vacancy has sixfold symmetry, [and hence for small q we expect $\vec{u}(\vec{q})$ to be isotropic], interstitials only have three- or twofold symmetry (see Figs. 2 and 3) and hence, $\vec{u}(\vec{q})$ is anisotropic. (Actually, the charge neutrality condition

$$u_\alpha(\vec{q}) \sim \frac{A_c q_\alpha}{|q|} \tag{2.39}$$

will still apply, and it is only in the next order in q that anisotropy will appear.) We will hence proceed no further in this section with analytical calculations, and will just quote results from the computer. We have calculated (in addition to the vacancy already discussed) the energies of two distinct stable interstitials and a divacancy.

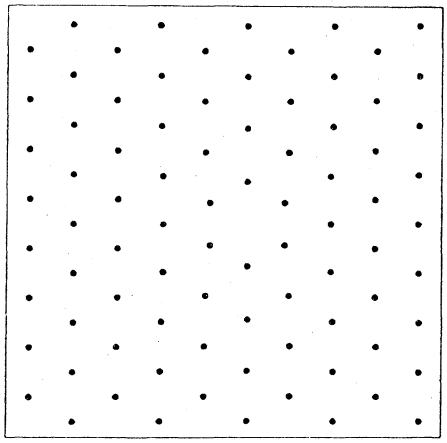

FIG. 1. Vacancy.

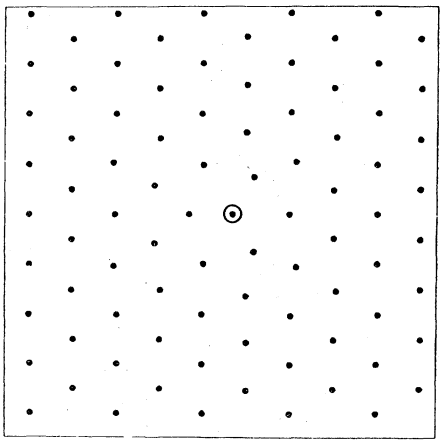

FIG. 2. Centered interstitial.

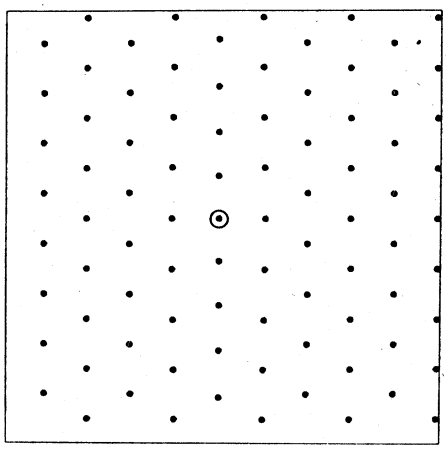

FIG. 3. Edge interstitial.

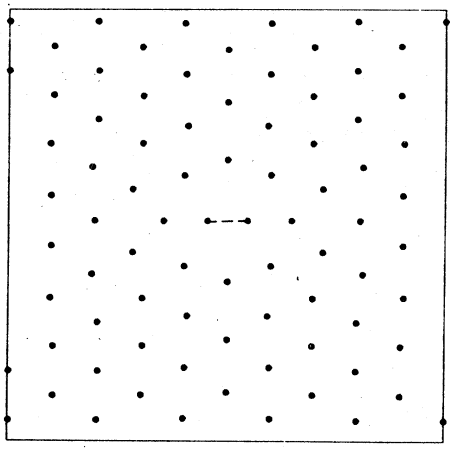

FIG. 5. Twisted bond.

The centered interstitial, Fig. 2, has energy

$$E_{CI}=0.15\epsilon_0 \ , \tag{2.40}$$

considerably lower than the vacancy energy. It should be noted that (as might be expected) the lattice distortions are considerably larger for the interstitials than for the vacancy. An at first surprising result is that the "edge interstitial," Fig. 3, which might be expected to be only a saddle point in the energy, is actually stable with a rather low energy

$$E_{EI}=0.125\epsilon_0 \ . \tag{2.41}$$

The divacancy, Fig. 4 shows a characteristic dipentagonal form and has an energy of

$$E_{DV}=0.25\epsilon_0 \tag{2.42}$$

In addition to these vacancies and interstitials, we here include computations of the energy of two other small defects which are only "saddle-point" configurations of the energy rather than minima. These are the "twisted bond" and "twisted triangle" (see Figs. 5 and 6) which may play a role in determining rates of particle exchange at finite temperatures (see Sec. V). They have energies of

$$E_{TB}=0.31\epsilon_0$$

and (2.43)

$$E_{TT}=0.27\epsilon_0 \ ,$$

respectively.

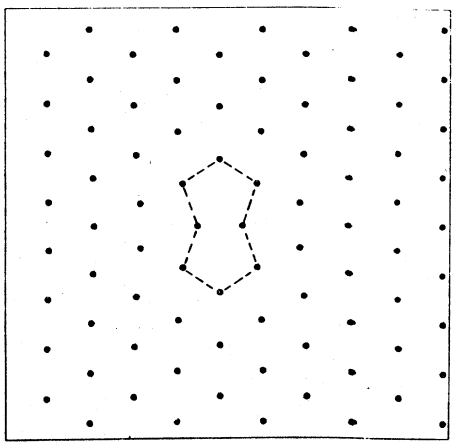

FIG. 4. Divacancy.

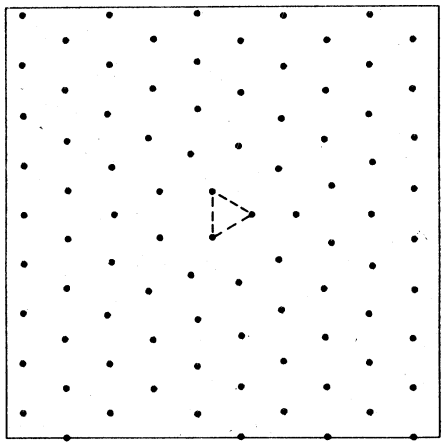

FIG. 6. Twisted triangle.

E. Effect of periodic boundary conditions

To rationalize our assumption that the interactions with the image vacancies, etc., can be ignored in the computation with periodic boundary conditions, we here consider the interaction between two vacancies, one at the origin and the other at a large distance $\vec{r}$. At large distances from either vacancy the distortion is small and will be given by the sum of the parts due to each vacancy

$$u_\alpha(\vec{q}) = \frac{iA_c q_\alpha}{q^2}(1+cq+dq^2)(1+e^{i\vec{q}\cdot\vec{r}}) \quad . \tag{2.44}$$

The interaction energy is then given by the cross term of $u\Pi u$

$$E^v_{\text{inter}} \propto -e^2 \int_{\vec{q}} \frac{2\pi}{q}[1+O(q)+O(q^2)]e^{i\vec{q}\cdot\vec{r}}$$

$$\propto -e^2 \int_0^{k_D} dq\, J_0(qr)\,[1+O(q)+O(q^2)]$$

$$= \frac{-e^2}{r} + O\left(\frac{1}{r^3}\right) \quad . \tag{2.45}$$

The order q term does not contribute since

$$\int_0^\infty q\, dq\, J_0(qr) = 0 \quad , \tag{2.46}$$

and there is an additional energy $+e^2/r$ from the Coulomb interaction between the two missing electrons which exactly cancels the $-e^2/r$ in Eq. (2.45). Hence, we find that the total interactioin energy between two vacancies goes as $1/r^3$ (the same result as continuum elasticity theory with finite μ and λ) and is presumably negligible for $r/a_0 \sim 30$.

The divacancies and interstitials also discussed in this section, can be considered to be composed of a pair of dislocations at one or two lattice spacings separation. In Sec. III it will be shown that the total energy change due to the images goes as a_0^2/L^2 and is hence again negligible. In fact, due to higher symmetry, the interactions between some of the small defects (e.g., vacancies, see above) fall off *faster,* i.e., as $1/r^3$.

III. DISLOCATIONS

The Kosterlitz-Thouless theory of two-dimensional melting[6–8] suggests that *dislocations* are responsible for the melting of two-dimensional solids. In this section we compare theoretical and numerical predictions for the energetics of dislocations.

In two dimensions, dislocations are point defects (the intersection of dislocation lines in three dimensions with the plane) characterized by a two-dimensional Burger's vector, $\vec{b}$, which is Bravais lattice vector of the two-dimensional lattice. A single dislocation in a system of area A has an energy which diverges as $\log(A/a_0^2)$ where a_0 is the lattice spacing. However, in a system with many dislocations, $\{\vec{b}_i\}$, the energy is finite as long as

$$\sum_i \vec{b}_i = 0 \quad . \tag{3.1}$$

This condition is analogous to charge neutrality in a Coulomb system.

For large separations between dislocations, we can write the total energy as the sum of pairwise interactions

$$E = \frac{1}{2}\sum_{i\neq j} E_0^d(\vec{r}_i - \vec{r}_j; \vec{b}_i, \vec{b}_j) + \sum_i E_c(b_i^2) \quad , \tag{3.2}$$

where the pair interaction E_0^d is given at separations $\vec{r}_{ij} \equiv \vec{r}_i - \vec{r}_j$ large compared to a_0 by continuum elasticity theory[9]

$$E_0^d(\vec{r}_{ij}; \vec{b}_i, \vec{b}_j) = \frac{K}{4\pi}\left[-\vec{b}_i\cdot\vec{b}_j \ln\left(\frac{|\vec{r}_{ij}|}{a_0}\right) + \frac{(\vec{b}_i\cdot\vec{r}_{ij})(\vec{b}_j\cdot\vec{r}_{ij})}{|\vec{r}_{ij}|^2}\right] + O\left(\frac{a_0}{r_{ij}}\right) \quad . \tag{3.3}$$

and we have lumped all local and nonlinear effects near the cores of the dislocations into a core energy $E_c(|b|^2)$ which increases with increasing $|b|$. We shall, in particular, be interested in dislocations with minimal Burger's vectors $|\vec{b}| = a_0$ and for simplicity denote this minimum core energy by

$$E_c \equiv E_c(a_0^2) \quad . \tag{3.4}$$

Dislocations with larger Burger's vectors are usually unstable to division into several dislocations with minimal Burger's vectors.

The coefficient K in Eq. (3.3) is given in terms of Lamé coefficients by

$$K = \frac{4\mu(\mu+\lambda)}{2\mu+\lambda} \quad . \tag{3.5}$$

For the electron case, $\lambda = \infty$, we have simply[10]

$$K = 4\mu \quad .$$

In this section we compare theoretical predictions for the energy of pairs of minimal dislocations with numerical calculations for electrons with periodic boundary conditions and thereby extract information on the core energy and the approach to the asymptotic form of the pairwise interaction given by Eq. (3.3).

A. Dislocations with periodic boundary conditions

In order to compare with our numerical computations with square periodic boundary conditions of period L, it is necessary to calculate the total energy per block of size $L \times L$ of an infinite square array of dislocation pairs with Burger's vectors $+\vec{b}$ and $-\vec{b}$. This energy, for pairs of separation $\vec{\rho}$, is given by

$$E = 2E_c + E_p^d(\vec{\rho}) \ , \tag{3.7}$$

where

$$E_p^d(\vec{\rho}) = E_0^d(\vec{\rho}) + \sum_{\vec{R}\neq 0} E_0^d(\vec{R}-\vec{\rho}) - E_0^d(\vec{R}) \tag{3.8}$$

the sum runs over $\vec{R} = (l_x L, l_y L)$ with l_x, l_y integers and

$$E_0^d(\vec{r}) = E_0^d(\vec{r}; \vec{b}_1 = \vec{b},\ \vec{b}_2 = -\vec{b}) = \frac{K}{4\pi}\left[b^2 \ln\left(\frac{|\vec{r}|}{a_0}\right) - \frac{(\vec{b}\cdot\vec{r})^2}{|\vec{r}|^2}\right] . \tag{3.9}$$

We note that, provided the sum in Eq. (3.8) is made convergent at large distances by an appropriate method, E_p^d will be periodic, i.e.,

$$E_p^d(\vec{R}+\vec{\rho}) = E_p^d(\vec{\rho}) \ , \tag{3.10}$$

and for $|\vec{\rho}| \ll L$, E_p^d clearly reduces to E_0^d. The sum in Eq. (3.8) is very badly behaved, however, and we need a method for making sense of it and evaluating it numerically. We use a generalization of the method, originally due to Ewald, which is extremely useful for calculating oscillating Coulomb Madelung energy summations.

To evaluate a sum of the form

$$\sum_{\vec{R}} f(\vec{R}-\vec{\rho}) \tag{3.11}$$

with $f(\vec{r})$ nonanalytic near $\vec{r}=0$ and with large contributions to the sum from large R, we divide (if possible) the function $f(\vec{r})$ into two parts

$$f(\vec{r}) = f_<(\vec{r}) + f_>(\vec{r}) \ , \tag{3.12}$$

with $f_<(\vec{r})$ decaying at large r as $e^{-\alpha r^2}$ (α is an arbitrary parameter to be fixed later) and $f_>(\vec{r})$ analytic near the origin. The sum of $f_<$ is now rapidly convergent and we are left with the problem of summing the ill-behaved series

$$\sum_{\vec{R}} f_>(\vec{R}-\vec{\rho}) \ . \tag{3.13}$$

It is now convenient to make use of the identity

$$\sum_{\vec{R}} f_>(\vec{R}-\vec{\rho}) = \frac{1}{L^2}\sum_{\vec{G}} e^{-i\vec{G}\cdot\vec{\rho}} f_>(\vec{G}) \ , \tag{3.14}$$

where $f_>(\vec{Q})$ is the Fourier transform of $f_>(\vec{r})$:

$$f_>(\vec{Q}) = \int d^2r\, e^{-i\vec{Q}\cdot\vec{r}} f_>(\vec{r}) \tag{3.15}$$

and $\vec{G}$ are "block reciprocal-lattice" vectors $\vec{G} = (2\pi/L)(g_x, g_y)$ with g_x, g_y integers. Now, however, since $f_>(\vec{r})$ is analytic near $\vec{r}=0$, $f_>(\vec{G}) \sim e^{-\beta G^2}$ for large G and hence the sum over $\vec{G}$ in Eq. (3.14) is rapidly convergent, and we can write

$$\sum_{\vec{R}} f(\vec{R}-\vec{\rho}) = \sum_{\vec{R}} f_<(\vec{R}-\vec{\rho}) + \frac{1}{L^2}\sum_{\vec{G}} e^{-i\vec{G}\cdot\vec{\rho}} f_>(\vec{G}) \ , \tag{3.16}$$

which is now explicitly periodic in $\vec{\rho}$. [The only ambiguity in Eq. (3.16) arises from the $\vec{G}=0$ term, which may be divergent or ill defined.]

The sum in Eq. (3.8) is actually of a slightly more complicated form than Eq. (3.11),

$$\sum_{\vec{R}} f(\vec{R}-\vec{\rho}) - \sum_{\vec{R}\neq 0} f(\vec{R}) \ , \tag{3.17}$$

with each sum separately infinite but the difference finite. It is straightforward to generalize Eq. (3.16) to

$$\sum_{\vec{R}} f(\vec{R}-\vec{\rho}) - \sum_{\vec{R}\neq 0} f(\vec{R}) = \sum_{\vec{R}\neq 0} [f_<(\vec{R}-\vec{\rho}) - f_<(\vec{R})] + \frac{1}{L^2}\sum_{\vec{G}\neq 0} (e^{-i\vec{G}\cdot\vec{\rho}} - 1) f_<(\vec{G}) + f_<(\vec{\rho}) \ . \tag{3.18}$$

Now the $\vec{G}=0$ term is absent from the sum. To evaluate Eq. (3.8) we now need to choose an appropriate $f_<$

$$f_<(\vec{r}) = \frac{K}{4\pi}\left[-b^2 \tfrac{1}{2}[E_1(\alpha r^2) + \ln\alpha + \gamma] - \frac{(\vec{b}\cdot\vec{r})}{r^2} e^{-\alpha r^2}\right] , \tag{3.19}$$

with

$$E_1(x) = -\mathrm{Ei}(-x) = \int_x^\infty \frac{e^{-t}}{t}\, dt \tag{3.20}$$

and γ Euler's constant. With this choice of $f_<$,

$$f_<(\vec{r}) = E_0^d(\vec{r}) - f_<(\vec{r}) \tag{3.21}$$

is analytic at $r=0$ and can be Fourier transformed to

obtain

$$f_<(\vec{Q}) = \frac{K}{4\pi}\frac{e^{-Q^2/4\alpha}}{Q^2} \times 4\pi\left[-b^2 + (\vec{b}\cdot\vec{Q})^2\left(\frac{1}{Q^2}+\frac{1}{4\alpha}\right)\right] . \quad (3.22)$$

If we choose $\alpha = \pi/L^2$ both sums in Eq. (3.18) converge equally rapidly and a few terms of each give accurate results.

The calculation described above gives the energy per pair of a periodic array of dislocation pairs in a large crystal with *free* boundary conditions (at constant pressure). In our numerical calculations, however, we have imposed periodic boundary conditions on the electrons in a fixed block whose size and shape were chosen to accommodate an integral number of cells of the original *defect-free* lattice, with essentially vanishing shear stress. Since this procedure will generally result in additional stresses in the defective sample, it is necessary to take account of the macroscopic stress energy, when comparing the numerical results with the analytic calculations.

The additional stresses resulting from enforcing periodic boundary conditions are of two kinds. The first is due to a change in the average density of particles caused by the removal or addition of part of a row between the two dislocations. This compressional (or expansional) effect is simply taken into account by the method described in the introduction in the same way as for vacancies, etc. However, for dislocations there is in addition a shear stress which cannot relax due to the periodic boundary conditions. This can most easily be seen if a whole horizontal row of electrons (corresponding to dislocations at boundaries of the unit block) is removed. In this case the system is again a regular lattice after relaxation; however the lattice spacing is different in different directions, and hence there is clearly an unrelaxed stress. While for an arbitrary pair of dislocations the situation is more complicated; the stress energy can be calculated as follows. Let U_{ij} denote the average distortion of the periodic block which would occur if the constraint of fixed size and shape were removed. The additional shear energy due to the imposed constraint of fixed (square) shape is then

$$E^s = \mu(U_{ij} - \tfrac{1}{2}\delta_{ij}U_{kk})^2\frac{1}{L^2} . \quad (3.23)$$

For a pair of dislocations of Burger's vectors $\pm\vec{b}$ at a separation $\vec{\rho}$, it can be shown that

$$U_{ij} = \tfrac{1}{2}(b_i\epsilon_{jl}\rho_l + b_j\epsilon_{kl}\rho_l) \quad (3.24)$$

and the shear energy is simply

$$E^s = \tfrac{1}{2}\mu b^2\frac{\rho^2}{L^2} \quad (3.25)$$

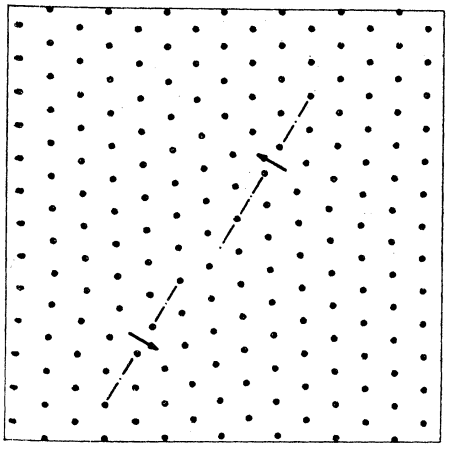

FIG. 7. Pair of dislocations. The dash-dotted lines show the axes of symmetry of the dislocations. The arrows indicate the Burger vectors, and are located so that the center of each arrow coincides with the position of the dislocation according to our definition.

independent of direction of $\vec{b}$ or $\vec{\rho}$. It is simple to check that this expression is correct for the case described above with one row removed.

Taking into account the effects of image dislocations, additional compression and additional shear, we can now compare theoretical and numerical calculations for the energy of various dislocation pairs to try and extract the core energy E_c. Before doing this we must define the position of a dislocation. Clearly this definition is somewhat arbitrary and we make what is a reasonably natural choice.

Consider dislocations in a triangular crystal, as shown in Fig. 7. In the regions of maximum distortion, there is a well-defined symmetry axis (dash-dotted lines) at 30° with respect to the unperturbed lattice. On that symmetry axis, the separation between the electrons is $a_0\sqrt{3}$, except for one pair which is separated by approximately a_0. We define the midpoint between these two electrons as the position of the dislocation. The Burger's vectors, which are perpendicular to the symmetry axes, are indicated by the arrows. For dislocation pairs separated by pure glide, this definition leads to separation vectors which are parallel to the Burger vectors, as they should be. Another dislocation pair, similar to a divacancy, but with a different symmetry, and also described by two missing particles, is shown in Fig. 8.

We now proceed with comparison of the energies of various dislocation pairs. In Table I data on various dislocations and theoretical and numerical values for their energies are presented. The average core energy based on nine different configurations of pairs

TABLE I. Dislocations. Summary of numerical and analytical results on energies of dislocation pairs with separations ρ and minimal Burger's vectors at an angle θ to their separation vectors: the numerically calculated energy in a system with periodic boundary conditions, (E^n), the energy from elastic theory excluding (E_0^d) and including (E_p^d) images, the additional energy (E^s) due to the shear caused by periodic boundary conditions, and the core energy (E_c) are tabulated in units of ϵ_0.

$\rho\ (a_0)$	θ	E^n	E_0^d	E_p^d	E^s	$E_c=\frac{1}{2}(E^n-E_p^d-E^s)$
6.7	86°	0.34	0.171	0.153	0.009	0.089
3.2	80°	0.31	0.102	0.098	0.002	0.105
9.8	88°	0.365	0.205	0.168	0.020	0.089
5.3	75°	0.30	0.143	0.131	0.006	0.082
2.5	44°	0.29	0.039	0.037	0.001	0.126
13.6	89°	0.465	0.234	0.168	0.038	0.130
8.6	81°	0.41	0.191	0.161	0.015	0.117
6.2	55°	0.393	0.134	0.119	0.008	0.133
2.5	46°	0.280	0.044	0.041	0.001	0.119

of dislocations is

$$E_c=(0.11\pm0.02)\epsilon_0\ . \tag{3.26}$$

The long distance form for the dislocation-dislocation interaction energy [Eq. (3.9)] is seen to be valid down to rather small distances, $\approx$3 lattice spacings.

In principle, vacancies and interstitials can be considered as dislocation pairs with separation one lattice spacing perpendicular to $\vec{b}$ (the "climb" direction), but since the former have a higher symmetry than the latter, it is more useful to consider them as separate entities. In particular, as a consequence of symmetry, the interaction between vacancies, as discussed in Sec. II falls off as $1/r^3$, while that between dislocation pairs $\sim 1/r^2$. In the present paper we will not consider a defect to be a dislocation pair unless the separation is *at least two lattice spacings.*

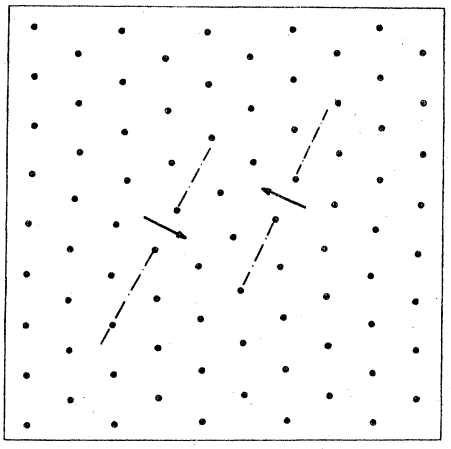

FIG. 8. Dislocation pair with two missing electrons, similar to a divacancy, but with different symmetry.

In addition, dislocation pairs separated in the direction *parallel* to $\vec{b}$ (the "glide direction") can be created without adding or removing particles. Pairs of this kind with one or two lattice spacing separation are almost certainly unstable, although they may be important for renormalization of the elastic constants (see Sec. V). We shall denote such pairs "virtual" dislocation pairs, and we shall thus impose the restriction that real dislocation pairs having $\vec{\rho}\parallel\vec{b}$ should be separated by at least three lattice spacings.

With the conventions adopted above, the minimum energy for a pair is estimated to be

$$2E_c+\frac{\mu}{\pi}(\ln 3-1)\simeq 2E_c+0.01\epsilon_0\approx 2.1E_c\ , \tag{3.27}$$

which is achieved for a separation of three lattice spacings in the glide direction.

IV. GRAIN BOUNDARIES

Another defect which partially destroys the ordered solid is the grain boundary, a line defect separating domains tilted with respect to each other by an angle θ.

A. Energy of grain boundaries (analytical)

Small angle grain boundaries can be considered as lines of dislocations with equal Burger's vectors $\vec{b}$.[11] The configuration of lowest energy is an equally spaced row of dislocations of minimal Burger's vectors perpendicular to the grain boundary. For definiteness, let us consider two parallel grain boundaries separated by a distance y, one consisting of N disloca-

tions of Burger's vectors in the y direction ($b_y = a_0, b_x = 0$) with separation $s >> a_0$, and the other identical but with Burger's vectors in the opposite direction [$b_y = -a_0$, see Fig. 9(a)]. (As discussed in Sec. III, for the overall energy to be finite, the total Burger's vector must be zero, hence the necessity for considering two equal but opposite grain boundaries.) The energy of this configuration can be calculated relatively straightforwardly and it is found that the total energy is[11]

$$\frac{E(y)}{N} = 2E_c + \frac{Ka_0^2}{4\pi}\left[\ln\frac{s}{2\pi a_0} - \frac{\pi y}{s}\coth\frac{\pi y}{s} + \ln 2 \sinh\frac{\pi y}{s}\right] . \quad (4.1)$$

For large separations y, we find that

$$\frac{E(\infty)}{N} - \frac{Ka_0^2 y}{2s} e^{-2\pi y/s} , \quad (4.2)$$

which drops off very rapidly for $Y \gtrsim s$.

By taking the limit $y \to \infty$ we find that the energy per unit lattice spacing for *one* grain boundary is

$$\epsilon = \frac{a_0 E(\infty)}{2Ns} = \frac{a_0}{s}E_c + \frac{Ka_0^2}{4\pi}\frac{a_0}{2s}\ln\frac{s}{2\pi a_0} . \quad (4.3)$$

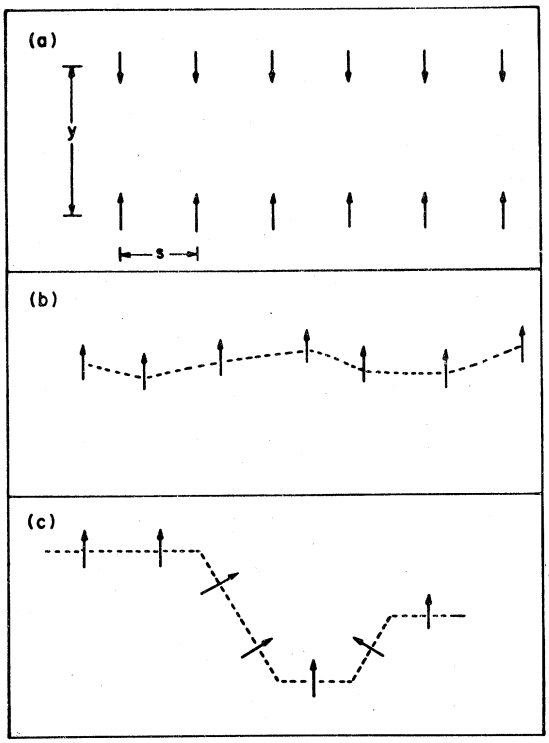

FIG. 9. Grain boundaries as lines of dislocations, depicted by their Burger's vectors: (a) two parallel grain boundaries, (b) "vibrating" small angle grain boundary, and (c) "meandering" large angle grain boundary.

Since the angle θ of the grain boundaries is just a_0/s for small angles, we find the well-known result[11]

$$\epsilon(\theta) \sim -\theta(\ln\theta + \text{const}) . \quad (4.4)$$

Clearly this form cannot be right for large angles, since we have not considered nonlinear effects other than those buried in the core energy, E_c. In particular, for a triangular lattice it is clear that $\epsilon(\theta)$ must be periodic in θ with a period of 60°. To obtain a reasonable form for $\epsilon(\theta)$, we guess a function which has the appropriate periodicity and is correct for small θ and hope that the result will be reasonably good even for $\theta \sim 30°$ (the maximum possible angle).

The simplest form with the required properties is obtained by replacing a_0/s in Eq. (4.2) by $\frac{1}{3}\sin 3\theta$;

$$\epsilon(\theta) \simeq \tfrac{1}{3}\sin 3\theta\left[E_c - \frac{Ka_0^2}{8\pi}\ln(\tfrac{2}{3}\pi \sin 3\theta)\right] . \quad (4.5)$$

For $\theta = 30°$ Eq. (4.3) yields

$$\epsilon(30°) = 0.029\epsilon_0 , \quad (4.6a)$$

which differs by a rather small amount from the result of Eq. (4.5).

$$\epsilon(30°) = 0.026\epsilon_0 . \quad (4.6b)$$

Before comparing this analytical result with numerical calculations, however, we must discuss additional complications. In a real crystal, even for small angle grain boundaries, the dislocations will not be exactly equidistant due to the discreteness of the underlying lattice. There will thus be a small contribution to the energy arising form deviations of the dislocation separations from their average values. This will give a correction to the energy per lattice spacing of order $(a_0/s)^3$, which is hence negligible for small angles.

For large angle grain boundaries, in addition to the nonlinear dislocation interactions which we have hidden in Eq. (4.5), there are again corrections due to the discreteness. Both of these effects are hard to estimate, but our computer simulations (see below) suggest they are small, possibly due to cancellation of many, more or less random, positive and negative contributions to the total energy.

B. Comparison with numerical computations

We have investigated numerically several straight, large angle grain boundaries (Figs. 10 and 11). The numerical results are summarized in Table II. Due to the periodic boundary conditions, we actually calculated the energy of a parallel array of grain boundaries with separation $y = 13a_0$. However, $2\pi y/s$ is very large and hence by [Eq. (4.2)] the interaction energy of a grain boundary with its images is negligible and can be ignored. For the large angle grain

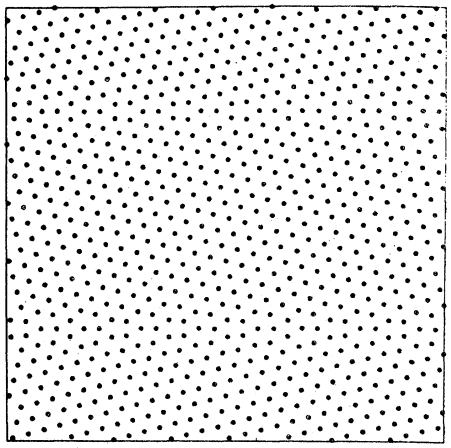

FIG. 10. Two straight-line 29.0° grain boundaries.

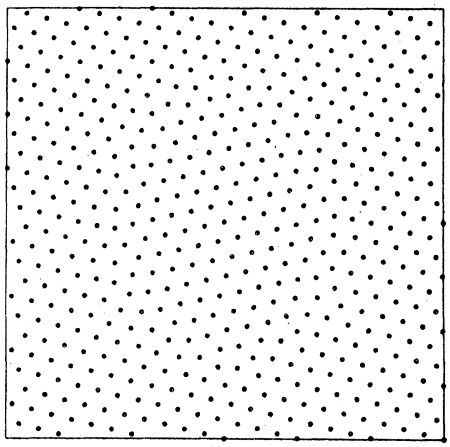

FIG. 12. Hexagonal 29.8° grain boundary of length $\sim 40a_0$.

boundaries investigated, we find slight variations in the energy of sets of grain boundaries with almost the same angle but different methods of preparation (e.g., sliding one half crystal slightly with respect to the other before relaxing the system). This is in accord with the expected effects of nonlinearities discussed above.

In addition to straight grain boundaries, we have investigated several roughly hexagonal domains (Figs. 12–14). The energies of these configurations are listed in Table II. The energy per lattice spacing of the boundary is roughly the same as that for a straight grain boundary. From this we can conclude that, at least on the scale of ten lattice spacings, the "corner" energy associated wtih bending a grain boundary is small. This will be important for the possibilities of grain boundary melting discussed in Sec. V.

To summarize, the energies per lattice spacing of length of the large angle grain boundaries considered with angles $22° < \theta < 30°$ lie in the range

$$0.0185\epsilon_0 < \epsilon < 0.0226\epsilon_0 \tag{4.7}$$

and are slightly lower than those given by the interpolation formula in Eq. (4.5). The discrepancies can presumably be attributed to the nonlinear effects discussed above.

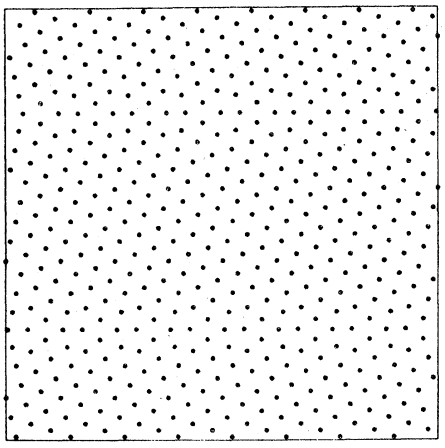

FIG. 11. Two straight-line 21.8° grain boundaries.

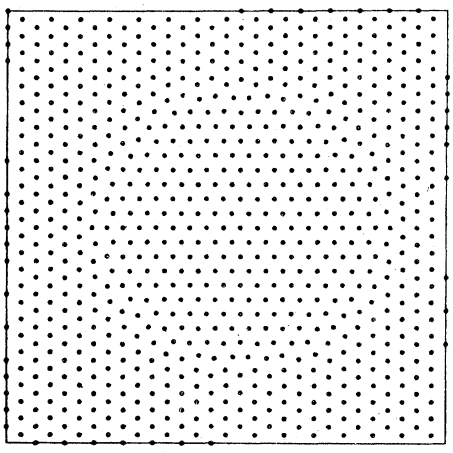

FIG. 13. Hexagonal 30° grain boundary with length $\sim 52a_0$.

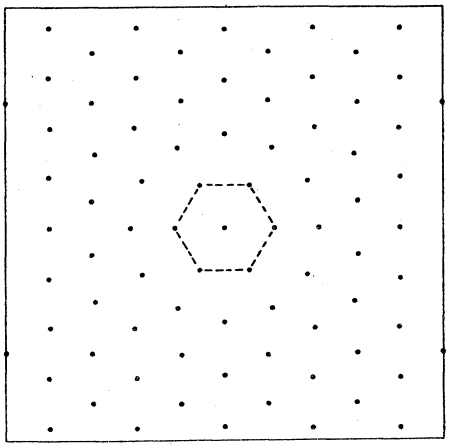

FIG. 14. Twisted hexagon. Can be regarded as hexagonal 30° grain boundary of length $\sim 10a_0$.

V. FINITE TEMPERATURES, DISCUSSION, AND CONCLUSIONS

So far in this paper all our calculations have been at zero temperature, yet, as was mentioned in the Introduction, an important motivation in studying defects is to understand properties of the electron solid at finite temperatures, and hopefully to learn something about the melting process. In this section, we shall briefly discuss several finite temperature properties. First, we review predictions of the dislocation theory of two-dimensional melting, in particular as applied to our system,[6–8] and mention the results of several computer simulations.[12–14] We next estimate densitites of various defects, which will affect the finite temperature behavior. We then consider grain boundaries as a possible mechanism for melting of the electron solid. Lastly, we discuss some dynamical properties of the solid.

A. Melting

It has been known for a long time that there can be no long-range translational order in two-dimensional systems of the type usually associated with a solid.[15] However, Kosterlitz and Thouless (KT)[6] have suggested that there can be a second-order transition from a liquid to a low-temperature "solid" phase characterized by the existence of a finite shear modulus. They predict that dislocations are present in the solid phase only in bound pairs, but above the transitions temperature, T_c, the system becomes unstable to the creation of free dislocations and melts. At the transition the shear modulus drops discontinuously to zero. KT further predict that the ratio of the combination of elastic constants discussed in Sec. III to the temperature approachs a universal constant at T_m (Ref. 7)

$$\lim_{T \to T_m^-} \frac{K(T) a_0^2}{T} = 16\pi \ , \tag{5.1}$$

where $K(T)$ is given in terms of the *finite temperature* Lamé coefficients $\mu(T)$ and $\lambda(T)$ by

$$K(T) = \frac{4\mu(T)[\mu(T)+\lambda(T)]}{2\mu(T)+\lambda(T)} \ . \tag{3.5'}$$

Thouless[10] has estimated the melting temperature of the electron system by using the *zero-temperature* values for μ and λ ($\lambda = \infty$) in Eqs. (3.5') and (5.1). He finds that in terms of the dimensionless parameter,

$$\Gamma = \frac{(\pi n_s)^{1/2} e^2}{T} \ , \tag{5.2}$$

T_m is given by

$$\Gamma_m^{\rm Th} = \Gamma(T_m^{\rm Th}) = 78.7 \ . \tag{5.3}$$

However, μ and λ are expected to be renormalized at finite temperature by nonlinear processes, in particular nonlinear phonons and dislocation pairs. Hence this prediction for Γ_m is at best a reasonable

TABLE II. Grain boundaries. Summary of results on grain boundary energies and the figure numbers in which they are illustrated: the length, angle (θ), numerical values for the total energy (E^n), and energy per length a_0 (ϵ^n) are tabulated in units of ϵ_0.

Type	Figure	θ	Length	$E^n(\epsilon_0)$	$\epsilon^n(\epsilon_0)$
Straight	10	21.8°	42	0.778	0.0185
Straight	11	29.8°	54	1.22	0.0226
Hexagon	12	27.8°	40	0.927	0.0232
Hexagon	13	30°	52	1.12	0.0215
Small hexagon	14	30°	≈ 10	0.26	~ 0.026

guess. Since $\mu(T)$, $\lambda(T)$, and hence T_m depend on renormalizations of μ and λ by dislocations (and probably other defects) it is useful to make some estimates of dislocation pair (and other defect) densities; these will enter any calculation of $\mu(T)$ and $\lambda(T)$.[6,7,13]

We first compare the Thouless estimate [Eq. (5.3)] for Γ_m to that found in the experiments and to several numerical calculations.

Grimes and Adams[2] find that the transition in electrons on helium mentioned earlier is well parametrized by $\Gamma(T_m)=\Gamma_m$ with

$$\Gamma_m^{\rm exp}\simeq 137\pm 15 \tag{5.4}$$

considerably larger (corresponding to lower temperatures) than $\Gamma_m^{\rm Th}$.

Three numerical simulations have been reported, two molecular dynamics (by Hockney and Brown[12] and very recently by Morf[13]) and a Monte Carlo calculation by Gann *et al.*[14] They find, respectively,

$$\Gamma_m^{\rm num}\simeq\begin{cases}95\pm 2\ , \\ 130\pm 10\ , \\ 125\pm 15\ . \end{cases} \tag{5.5}$$

While the latter two results are in reasonable agreement with the experiment, the result by Hockney and Brown differs considerably. They find λ-like behavior of the specific heat at $\lambda\sim 95\pm 2$ and identify this as the melting transition. As discussed in Ref. 13, we believe that their calculation is likely to suffer from nonequilibrium effects. It is, however, conceivable that some of the anomalies observed in their simulation might reflect the existence of the second phase transition conjectured by Halperin and Nelson[7] in which the orientational order of the "hexatic" (liquid-crystal) phase is lost due to the unbinding of disclinations. Since the orientational order parameter has not been determined in the calculation by Hockney and Brown,[12] no definite conclusions can be drawn.

The large difference between the Thouless estimate[10] for Γ_m and the experimental and numerical results[13,14] have been discussed in detail by Morf.[13] In his numerical simulations Morf found that, at low temperatures, the shear modulus decreases linearly with increasing T. At a value $\Gamma\sim 140$, this decrease amounts to approximately 22%. It is attributed to the effects of phonon-phonon interactions.[16] Using the renormalization-group equations derived by Halperin and Nelson,[7] Morf was able to estimate the additional renormalization of the shear modulus μ below the melting point due to the effects of dislocations. A linear extrapolation of the low-temperature shear modulus $\mu_L(T)$ was used as the initial value of the shear modulus, prior to renormalization by dislocation pairs. In addition, it was assumed that the dislocation core free energy $E_c(T)$ is reduced by phonon interactions in the same proportion as the shear modulus, i.e.,

$$E_c(T)/E_c(0)=\mu_L(T)/\mu_L(0)\ .$$

Using a value $E_c(0)=0.1\epsilon_0$ [which is 10% lower than the value given by Eq. (3.26) and which was obtained using a slightly different definition of the dislocation position], Morf obtained a melting point $\Gamma_m=128.2$ consistent with the strong drop of μ for $140>\Gamma>120$ observed in the simulation. This analysis shows that the large difference between the Thouless estimate[10] $\Gamma_m^{\rm Th}=78.7$ and the experimental and numerical results $\Gamma_m\sim 130$ does not rule out the validity of the theory of dislocation mediated melting in two dimensions; about half of the difference is explained by the renormalization of the shear modulus by phonon interactions and the other half by the effects of dislocations. A conclusive test of the validity of this theory, however, requires a much more accurate determination of the shear modulus at temperatures just below melting. Since such a conclusive test has not yet been carried out, it is interesting to discuss other possible mechanisms for melting in two dimensions. This will be done later in this section.

B. Defect densities

Let us first discuss the density of dislocation pairs as a function of temperature. This can be crudely estimated by treating the pairs of dislocations as diatomic molecules which do not interact with each other. As discussed in Sec. III, we will only count pairs with separation larger than $r_{\rm min}\approx 3a_0$. The number density of dislocation pairs per unit cell is easily found to be

$$e^{-2E_c/T}Z(\bar{K})\ , \tag{5.6}$$

where

$$\bar{K}=\frac{Ka_0^2}{T} \tag{5.7}$$

and Z is the internal partition function of a dislocation pair

$$Z(\bar{K})=3\int_{r>r_{\rm min}}\frac{d^2r}{A_c}\exp\left[-\frac{\bar{K}}{4\pi}\left[\ln\frac{r}{a_0}-\frac{(\hat{b}\cdot\vec{r})^2}{r^2}\right]\right]$$
$$=\frac{4\pi\sqrt{3}}{\bar{K}/4\pi-2}\left[\frac{r_{\rm min}}{a_0}\right]^{2-\bar{K}/4\pi}I_0\left[\frac{\bar{K}}{8\pi}\right]e^{\bar{K}/8\pi}\ , \tag{5.8}$$

where the factor of 3 comes from possible orientations of the Burger vectors and I_0 is a modified Bessel function. It is not clear what value of $K(T)$ should be used in evaluating Eq. (5.8). Probably the most appropriate would be to include phonon renor-

TABLE III. Defect densities. Densities per unit cell for several defects at three values of Γ. Columns headed A are derived using zero-temperature values for μ and E_D. Those headed B are derived using zero-temperature values scaled by $\mu_L(T)/\mu_L(0)$ (see text).

Defect	Density/unit cell					
	Γ = 120		Γ = 150		Γ = 200	
	A	B	A	B	A	B
Vacancy	8.8×10^{-8}	5.1×10^{-6}	1.5×10^{-9}	8.8×10^{-8}	1.8×10^{-12}	1.0×10^{-10}
Centered interstitial	7.8×10^{-5}	9.8×10^{-4}	6.2×10^{-6}	7.8×10^{-5}	9.0×10^{-8}	1.1×10^{-6}
Edge interstitial	6.3×10^{-4}	5.2×10^{-3}	7.7×10^{-5}	6.3×10^{-4}	2.3×10^{-6}	1.9×10^{-5}
Dislocation pairs	6×10^{-5}	4×10^{-3}	1.2×10^{-6}	6×10^{-5}	1.8×10^{-9}	9×10^{-8}

malizations (and possibly those from virtual dislocation pairs) in μ and λ but not renormalizations due to dislocation pairs.

In Table III we have tabulated estimates for the densities per unit cell of dislocation pairs and various other localized defects for three typical temperatures, Γ = 120, 150, and 200. For each temperature we list two values. The first is obtained by using the zero-temperature values for the defect energy, E_D, and the shear modulus. The second value is obtained by using a shear modulus, $\mu_L(T)$ (found in Morf[13]), which decreases linearly with temperature as discussed above. In addition, the defect energy is assumed to depend linearly on temperature, i.e.,

$$E_D(T)=E_D(0)\mu_L(T)/\mu_L(0) \ .$$

C. Grain boundaries and melting

In addition to the instability of two-dimensional (2-D) solids to formation of free dislocations exploited in the KT theory,[6] 2-D solids can also be unstable to formation of grain boundaries.

We consider here possible instabilities to formation of both small and large angle grain boundaries separately. There are two variations in the minimum energy form of a grain boundary [as in Fig. 9(a)] that we must consider at finite temperatures. The first of these is "vibration" [illustrated in Fig. 9(b)], in which the Burger vectors of the dislocations making up the grain boundary remain parallel but fluctuate in position.

The second in "meandering" [illustrated in Fig. 9(c)], in which the direction of the grain boundary and the burger vectors of its composite dislocations vary along the boundary in multiples of 60°.

We first consider a small angle grain boundary for which it easily can be shown that the dominant contribution to the entropy comes from "vibration", and second a large angle grain boundary whose fluctuations can mostly be described by "meandering".

If the small angle grain boundary is made up of parallel Burger's vectors with separation s, we showed in Sec. IV that its energy per lattice spacing of length is

$$\epsilon=\frac{a_0}{s}\left(\frac{Ka_0^2}{8\pi}\ln\frac{s}{a_0}+\text{const}\right) \ , \tag{5.9}$$

where the constant is independent of s/a_0 for $s \gg a_0$. We now allow each dislocation to deviate from its equilibrium position (equally spaced) by an amount $\vec{\rho}_n$, where n labels the dislocation. The total energy for a grain boundary of N dislocations is then

$$E_{\rm gb}=N\frac{s}{a_0}\epsilon+V_{\rm gb}\left(\frac{\vec{\rho}_n}{s}\right) \ , \tag{5.10}$$

where $V_{\rm gb}$ is the change in energy due to the displacement of the dislocations. The free energy is

$$F_{\rm gb}=N\frac{s}{a_0}\epsilon-T\ln\left\{\prod_n\int d^2\rho_n\, A_c^{-1}\exp\left[-\beta V_{\rm gb}\left(\frac{\vec{\rho}_n}{s}\right)\right]\right\}$$

$$=N\frac{Ka_0^2}{8\pi}\ln\left(\frac{s}{a_0}\right)-2NT\ln\left(\frac{s}{a_0}\right)+Nf \ , \tag{5.11}$$

where f is independent of s/a_0. For small angles ($s \gg a_0$) this will change sign at

$$T=\frac{Ka_0^2}{16\pi} \ , \tag{5.12}$$

which is identical to the KT calculation for the instability temperature to formation of free dislocations and, in fact, is essentially the same mechanism under a different guise.

The expression derived by Halperin and Nelson[7] for the correlations in the Burger vector density in the hexatic phase, $T > T_m$, shows an angular depen-

dence, which one may describe as a strong tendency for dislocations to arrange themselves is small angle grain boundaries.

While the instability of a 2-D solid to formation of small angle grain boundaries depends only on long-distance properties, our second example, instability to large angle grain boundaries depends on details of short-range interactions.

We consider an extremely oversimplified model of a meandering 30° grain boundary made of segments of roughly two lattice spacing (the separation between dislocations in a straight 30° grain boundary is $a_0/2\sin 15° \simeq 1.9a_0$) whose orientaiton varies along the grain boundary in steps of 60°. Each segment has an energy $2\epsilon(30°) \simeq 0.44\epsilon_0$ and a Burger vector perpendicular to it [Fig. 9(c)] and at the end of each we allow three possibilites: the grain boundary can continue in the same direction costing no energy, or it can bend 60° to the right of left costing an energy ϵ_c. If we ignore interactions between segments and the gain or loss of energy due to self-crossings, then our meandering boundary has a free energy per segment

$$F_{\rm gb} = 2\epsilon(30°) - T\ln(1+2e^{-\epsilon_c/T}) \ . \tag{5.13}$$

If ϵ_c is small, as it appears to be in practice (see Sec. IV), we can estimate a grain boundary melting temperature

$$T_c^{\rm gb} \simeq \frac{2\epsilon(30°)}{\ln 3} \tag{5.14}$$

(corresponding to $\Gamma_c^{\rm gb} \simeq 44$) above which the solid becomes unstable to large angle grain boundaries. While this estimate is a factor of two higher than $T_m^{\rm Th}$ and even larger compared to $T_m^{\rm num}$ and $T_m^{\rm exp}$ it is possible that entropy contributions from softening of vibrational modes near the grain boundary and self-crossing terms may lower the estimate of $T_c^{\rm gb}$ considerably. Thus, from the above estimates it appears unlikely, but still possible, that the experimentally and numerically observed melting at $\Gamma \sim 130$ is due to large angle grain boundary formation.

D. Dynamics

Thus far we have restricted ourselves to static quantities, we now briefly discuss several dynamic properties of the electron solid: interstitial diffusion, particle diffusion, and dislocation motion.

Because of their relatively low energy (see Sec. III) and hence reasonably high density, interstitials might be expected to play an important role in dynamical processes in the Wigner crystal. In addition, since the energy of an edge and centered interstitial are rather close, it is natural to guess that the barrier for interstitial motion, Δ_I, is low, possibly only of the order of the temperature for $\Gamma \sim \Gamma_m$. The interstitial diffusion constant, D_I, will be roughly given by

$$D_I \sim e^{-\Delta_I/T}\omega_0 a_0^2 \ , \tag{5.15}$$

where ω_0 is a characteristic microscopic vibration frequency

$$\omega_0 \sim 10^{11}\,\sec^{-1}\left(\frac{n_s}{10^8/\text{cm}^2}\right)^{3/4} \ . \tag{5.16}$$

For temperatures near T_c, D_I will be very large since $e^{-\Delta_I/T} \sim 1$.

The diffusion rate for a tagged electron, D, will have a contribution from interstitial diffusion as well as from two or more particle interchange

$$D \sim D_I\rho_I + \omega_0 a_0^2 e^{-\Delta_{\rm ex}/T} \ , \tag{5.17}$$

where ρ_I is the number density of interstitials (see Table III) and $\Delta_{\rm ex}$ is the barrier to particle interchange. If $\Delta_{\rm ex}$ is of the order of the energy of the twisted bond or triangle, which approximate the barrier heights for exchange (see Sec. II) then particle diffusion will be dominated by interstitial diffusion, the first term in Eq. (5.17).

Dislocation motion is of two sorts; motion parallel to the Burger vector, or glide, and motion perpendicular to the Burger vector, or climb. Glide involves no change in particle number and hence can proceed rapidly at microscopic rates characterized by ω_0. Dislocation climb, on the other hand, involves a change in the number of electrons (i.e., addition or subtraction of an electron in a half row terminating at the dislocation) and hence must proceed by absorption or emission of vacancies or interstitials. Assuming that this also is dominated by interstitials at least at temperatures of the order of T_c, the rate for climbing one lattice spacing will be of the order of $\omega_0\rho_I$, orders of magnitude slower than the rate for glide, even at relatively high temperatures.

All these estimates of rates of dynamical processes should be taken as rough, as large phonon fluctuations at moderate temperatures will probably enhance them considerably.

ACKNOWLEDGMENTS

The authors wish to acknowledge stimulating conversations with David R. Nelson and Annette Zippelius. This work has been supported in part by the National Science Foundation through the Harvard Materials Research Laboratory, through Grant No. DMR 77-10210, and through a fellowship to D.S.F. One of us (R.H.M.) wishes to acknowledge financial support by the Swiss National Science Foundation through Fellowship No. 82.528.0.77.

APPENDIX: NUMERICAL METHODS

In this appendix we describe the numerical methods employed for calculating defect energies. In the first section we present some general considerations about the required system size. Appendix section 2 is devoted to a description of the numerical methods for calculating energies and forces. In Appendix section 3 we describe the method for generating defects and we conclude the appendix with a discussion of the numerical errors of this calculation.

1. Choice of system size

Our goal is to calculate the energy of defects in an infinite system. As has been discussed in Sec. I, we do this by numerically calculating the energy of a defect in a finite system subject to periodic boundary conditions and choose the system large enough that the interaction of the defect with its periodic images can either be neglected or calculated by means of linear elasticity theory.

In order to be able to study the interactions between dislocations, we considered a system of between 20×20 and 30×30 particles as the minimum required size. For reasons of simplicity, we choose a square cell with 26×30 particles. This particular choice is motivated by the fact that the ratio between height and edge length of a symmetrical triangle is approximated by the rational fraction $\frac{13}{15}$ with an accuracy of 0.07%.

2. Calculation of energy and forces

The interaction energy $\phi(\vec{r}_i - \vec{r}_j)$ between an electron at position $\vec{r}_i$ and one at position $\vec{r}_j$ together with its image at positions $\vec{r}_j + \vec{\mathcal{R}}$ is given by

$$\phi(\vec{r}_i - \vec{r}_j) = \frac{2\pi e^2}{L^2} \sum_{\vec{\mathcal{G}} \neq 0} \frac{e^{i\vec{\mathcal{G}}\cdot(\vec{r}_i - \vec{r}_j)}}{\mathcal{G}} , \qquad \text{(A1)}$$

where L^2 is the system area and $\mathcal{G}$ are vectors of the square lattice reciprocal to the lattice of image points $\{\vec{\mathcal{R}}\} = \{(l_x L, l_y L)\}$. Since the system is in a uniform positive background, the term $\vec{\mathcal{G}} = 0$ has to be omitted in the summation.

For a numerical calculation Eq. (A1) is not suitable and we have to make use of the Ewald method. This leads to

$$\phi(\vec{r}) = \frac{2\pi}{L^2} \sum_{\vec{\mathcal{G}} \neq 0} \frac{\operatorname{erfc}(\mathcal{G}\kappa)}{\mathcal{G}} e^{i\vec{\mathcal{G}}\cdot\vec{r}} + \sum_{\vec{\mathcal{R}}} \frac{\operatorname{erfc}(|\vec{r} - \vec{\mathcal{R}}|/2\kappa)}{|\vec{r} - \vec{\mathcal{R}}|} - \frac{4\pi^{1/2}\kappa}{L^2} , \qquad \text{(A2)}$$

where $\operatorname{erfc}(x) = 1 - \operatorname{erf}(x)$ is the complementary error function and κ is a parameter which can be adjusted for optimal convergence. (Cf. Sec. III above where we discuss the Ewald method applied to the interaction between a dislocation pair and its images, mediated by the strain field of the crystal.) In terms of $\phi(\vec{r})$ the total energy E of our system with N particles may then be written

$$E = \frac{1}{2} \sum_{i,j=1}^{N} \left[\phi(\vec{r}_i - \vec{r}_j) - \delta_{ij} \frac{e^2}{|\vec{r}_i - \vec{r}_j|} \right] . \qquad \text{(A3)}$$

Here, in order to obtain the proper contribution from the interaction of an electron with its own images, the term $i = j$ must be treated as a limiting value, i.e.,

$$\lim_{\vec{r} \to 0} \left[\phi(\vec{r}) - \frac{e^2}{|\vec{r}|} \right] .$$

Even with the use of tabulated values for $\phi(\vec{r})$ and interpolation for the required separations $\vec{r}_i - \vec{r}_j$, the summation in Eq. (A3) requires an extremely large amount of computation (for 780 particles there are over 300 000 terms). For this reason we make use of an approximate method. We use a modified version of a mesh method described by Hockney *et al.*[17]

Let us describe our method in detail. First, we decompose the sum in Eq. (A3) into two parts: a contribution from nearby particles and one from further distant ones. Introducing a cutoff radius $\mathcal{R}_c$, we write Eq. (A3) in the form

$$E = \frac{1}{2} \sum_{\vec{\mathcal{R}}} \sum_{\substack{i \neq j \\ |\vec{r}_i - \vec{r}_j + \vec{\mathcal{R}}| < R_c}} \frac{e^2}{|\vec{r}_i - \vec{r}_j + \vec{\mathcal{R}}|} + \frac{1}{2} \sum_{i,j=1}^{N} \hat{\phi}(\vec{r}_i - \vec{r}_j) , \qquad \text{(A4)}$$

where

$$\hat{\phi}(\vec{r}) = \phi(\vec{r}) - \sum_{\substack{\vec{\mathcal{R}} \\ |\vec{r} + \vec{\mathcal{R}}| < R_c}} \frac{1}{|\vec{r} + \vec{\mathcal{R}}|} . \qquad \text{(A5)}$$

Like $\phi(\vec{r})$, $\hat{\phi}(\vec{r})$ is periodic in the "big" lattice $\{\vec{\mathcal{R}}\}$ and apart from its discontinuity at the cutoff radius R_c it is a smooth function of $\vec{r}$ which can be interpolated. While the first term in Eq. (A4) which contains $O(N)$ summations will be calculated exactly, the second (long-range) part, whose numbers of terms is $O(N^2)$, will be treated in an approximate way, which will involve only $O(N \ln N)$ operations. For this purpose, we introduce a square mesh with $M \times M$ points and with a square mesh unit cell of length $\Delta = L/M < R_c$. The mesh points will be denoted by $\vec{r}_{lm} = (l\Delta, m\Delta)$.

The idea of this mesh method is as follows. Consider two electrons at positions $\vec{r}_1$ and $\vec{r}_2$, separated by a distance greater than R_c. Let us denote the four mesh points closest to $\vec{r}_i$ by $\vec{\mathcal{P}}_i^{(k)} = (x_i^{(k)}, y_i^{(k)})$ $(k = 1, 2, 3, 4)$, which are the corners of the square

cell in which electron i lies. We now approximate the true interaction $\hat{\phi}(\vec{r}_1-\vec{r}_2)$ by a sum over interactions between suitably chosen partial "charges" $e_1^{(k)}$ at positions $\vec{\mathcal{P}}_1^{(k)}$ and corresponding ones $e_2^{(l)}$ at positions $\vec{\mathcal{P}}_2^{(l)}$:

$$\hat{\phi}(\vec{r}_1-\vec{r}_2)=\sum_{k=1}^{4}\sum_{l=1}^{4}e_1^{(k)}e_2^{(k)}\hat{\phi}(\vec{\mathcal{P}}_1^{(k)}-\vec{\mathcal{P}}_2^{(l)})+R \quad , \tag{A6}$$

where R stands for the remainder term. By choosing the partial "charges" $e_1^{(k)}$ in such a way that their associated dipole moment $\vec{p}_i=\sum_{k=1}^{4}e_i^{(k)}(\vec{\mathcal{P}}_i^{(k)}-\vec{r}_i)$ with respect to the electron position $\vec{r}_i$ vanishes, and that $\sum_{k=1}^{4}e_i^{(k)}=1$, the remainder term depends on second- and higher-order derivatives of $\hat{\phi}$ only and is of order Δ^2. This condition is satisfied by defining

$$e_i^{(k)}=(1-|x_i-x_i^{(k)}|\Delta^{-1})\,(1-|y_i-y_i^{(k)}|\Delta^{-1}) \quad . \tag{A7}$$

The approximation for $\hat{\phi}(\vec{r}_1-\vec{r}_2)$ provided by Eqs. (A6) and (A7) can be viewed as a linear interpolation formula, written in a form which is symmetrical under electron interchange.

We now define a mesh charge density

$$\hat{\rho}(\vec{r})=\sum_{i=1}^{N}\sum_{k=1}^{4}e_i^{(k)}\delta(\vec{r}-\vec{\mathcal{P}}_i^{(k)}) \quad , \tag{A8}$$

which is nonzero on mesh points $\vec{r}_{lm}$ only and which we can define periodic in the "big lattice", i.e.,

$$\hat{\rho}(\vec{r}+\vec{\mathcal{R}})=\hat{\rho}(\vec{r}) \quad .$$

Using the representation (A6) for $\hat{\phi}(\vec{r}_1-\vec{r}_2)$, Eq. (A4) for the energy may be written in the form

$$E=\sum_{\substack{\vec{\mathcal{R}}\\ |\vec{r}_i-\vec{r}_j+\vec{\mathcal{R}}|<R_c}}\frac{e^2}{|\vec{r}_i-\vec{r}_j+\vec{\mathcal{R}}|}+\frac{1}{2}\sum_{i=1}^{N}\sum_{k=1}^{4}e_i^{(k)}\sum_{l,m=1}^{M}\hat{\rho}(\vec{r}_{lm})\hat{\phi}(\vec{\mathcal{P}}_i^{(k)}-\vec{r}_{lm})+\Sigma_c+R' \quad , \tag{A9}$$

where the remainder term R', which will be neglected, is again of order $O(\Delta^2)$. The contribution Σ_c arises from electron pairs whose separation $|\vec{r}_i-\vec{r}_j+\vec{\mathcal{R}}|$ is close to R_c, such that some of the "partial charges" are separated by a distance larger than R_c and others by a distance smaller than R_c. It may be written

$$\Sigma_c=\tfrac{1}{2}e^2\sum_{i\neq j}\sum_{\vec{\mathcal{R}}}\sum_{k,l=1}^{4}\frac{e_i^{(k)}e_j^{(l)}}{a_{ij}^{(k,l)}}[\Theta(b_{ij}-R_c)\Theta(R_c-a_{ij}^{(k,l)})-\Theta(R_c-b_{ij})\Theta(a_{ij}^{(k,l)}-R_c)] \quad , \tag{A10a}$$

with

$$a_{ij}^{(k,l)}=|\vec{\mathcal{P}}_i^{(k)}-\vec{\mathcal{P}}_j^{(l)}+\vec{\mathcal{R}}| \tag{A10b}$$

and

$$b_{ij}=|\vec{r}_i-\vec{r}_j+\vec{\mathcal{R}}| \quad . \tag{A10c}$$

By $\Theta(x)$ we denote the Heaviside step function

$$\Theta(x)=0, \quad x<0 \quad ,$$

$$\Theta(x)=1, \quad x\geq 0 \quad .$$

Since only electron pairs whose separations (modulo $\vec{\mathcal{R}}$) lie in the interval $[R_c-2(2^{1/2})\Delta, R_c+2(2^{1/2})\Delta]$ can give rise to a contribution to Σ_c, the number of individual terms in Σ_c is of $O(N)$ and can be calculated in an efficient way simultaneously with the first term in Eq. (A9). The particular advantage of our approximation (A9) for the energy E lies in the fact that in this form the long distance contribution can be calculated efficiently making use of the fast-Fourier transform method. The convolution sum

$$\psi(\vec{r}_{ij})=\sum_{l,m=1}^{M}\hat{\rho}(\vec{r}_{lm})\hat{\phi}(\vec{r}_{ij}-\vec{r}_{lm}) \quad , \tag{A11}$$

which may be viewed as the electrostatic potential at $\vec{r}_{ij}$ due to the charges $e_i^{(k)}$ at mesh points $\vec{\mathcal{P}}_i^{(k)}+\vec{\mathcal{R}}$, is required only on mesh points $\vec{r}_{ij}$. Equation (A11) can be written

$$\psi(\vec{r}_{ij})=\frac{1}{M^2}\sum_{\vec{g}}e^{-2\pi i\vec{g}\cdot\vec{r}_{ij}}\tilde{\rho}(\vec{g})\tilde{\phi}(-\vec{g}) \quad , \tag{A12}$$

where $\vec{g}$ are the M^2 vectors of the lattice reciprocal to the mesh vectors $\vec{r}_{ij}$ and $\tilde{\rho}$ and $\tilde{\phi}$ are the discrete Fourier transforms of $\hat{\rho}$ and $\hat{\phi}$, defined by

$$\tilde{\rho}(\vec{g})=\frac{1}{M^2}\sum_{\vec{r}_{ij}}e^{2\pi i\vec{g}\cdot\vec{r}_{ij}}\hat{\rho}(\vec{r}_{ij}) \tag{A13}$$

and

$$\tilde{\phi}(\vec{g})=\frac{1}{M^2}\sum_{\vec{r}_{ij}}e^{2\pi i\vec{g}\cdot\vec{r}_{ij}}\hat{\phi}(\vec{r}_{ij}) \quad . \tag{A14}$$

For a given mesh size and cutoff R_c, $\tilde{\phi}(\vec{g})$ can be calculated once and forever. Using the fast-Fourier transform method, the number of operations required for the calculation of $\tilde{\rho}(\vec{g})$ and $\psi(\vec{r}_{ij})$ is $O(M^2(\ln M+\text{const}))$. Since for fixed accuracy of the energy per particle, the required number of mesh points M^2 increases like the number of particles N, we conclude from this that the total number of operations required for the computation of E using

Eqs. (A7)–(A10) and (A12)–(A14) requires $O(N(\ln N + \text{const}))$ operations, which was the goal of this method.

Let us now turn to the calculation of the forces $\vec{F}_i$ acting on the electrons i in an unrelaxed configuration. By differentiation of Eq. (A4) we get

$$\vec{F}_i = e^2 \sum_{\substack{j=1 \\ j\neq i}} \sum_{\substack{\vec{R} \\ |\vec{r}_i - \vec{r}_j + \vec{R}| < R_c}}^{N} \frac{\vec{r}_i - \vec{r}_j + \vec{R}}{|\vec{r}_i - \vec{r}_j + \vec{R}|^3} - \sum_{\substack{j=1 \\ j\neq i}} \vec{\nabla}_i \hat{\phi}(\vec{r}_i - \vec{r}_j) \tag{A15}$$

Using the mesh method, this can be written

$$\vec{F}_i = \vec{F}_i^{(s)} - \sum_{k=1}^{4} e_i^{(k)} \vec{\nabla} \psi(\vec{\mathcal{P}}_i^{(k)}) + \vec{\Sigma}_i^1 + R'' \ , \tag{A16}$$

where the first term in Eq. (A15) is denoted by $\vec{F}_i^{(s)}$ and $\vec{\Sigma}_i^1$ is the term corresponding to Σ_c in Eq. (A9) arising from the discontinuity of $\hat{\phi}(\vec{r})$ at the cutoff R_c. The remainder term is again of $O(\Delta^2)$, but now it is determined by the third derivative of $\hat{\phi}(\vec{r})$. To this order, $\vec{\nabla}\psi$ can be calculated by means of the finite difference approximation

$$\left.\frac{\partial \psi}{\partial x}\right|_{\vec{\mathcal{P}}_i^{(k)}} = \frac{1}{2\Delta} |(\vec{\mathcal{P}}_i^{(k)} + \Delta \vec{e}_x) - \psi(\vec{\mathcal{P}}_i^{(k)} - \Delta \vec{e}_x)| + O(\Delta^2) \tag{A17}$$

and

$$\left.\frac{\partial \psi}{\partial y}\right|_{\vec{\mathcal{P}}_i^{(k)}} = \frac{1}{2\Delta} |\psi(\vec{\mathcal{P}}_i^{(k)} + \Delta \vec{e}_y) - \psi(\vec{\mathcal{P}}_i^{(k)} - \Delta \vec{e}_y)| + O(\Delta^2) \ , \tag{A18}$$

where $\vec{e}_x$ and $\vec{e}_y$ are unit vectors in x and y direction.

If the calculation of the forces is done together with the calculation of the energy, this method does not require the computation of additional Fourier transforms.

The term $\vec{\Sigma}_i' = (\Sigma_{i,x}', \Sigma_{i,y}')$, which arises from pairs of particles with separation close to the cutoff radius R_c is given by

$$\Sigma_{i,n}' = \frac{e^2}{2\Delta} \sum_{\substack{j=1 \\ j\neq i}} \sum_{\vec{R}} \sum_{k,l=1}^{4} \sum_{\delta=\pm\Delta} \frac{e_i^{(k)} e_j^{(l)} \delta}{a_{ij}^{(k,l)}(\delta)} [\Theta(R_c - b_{ij})\Theta(a_{ij}^{(k,l)}(\delta) - R_c) - \Theta(b_{ij} - R_c)\Theta(R_c - a_{ij}^{(k,l)}(\delta))] \ , \tag{A19a}$$

where

$$a_{ij}^{(k,l)}(\delta) = |\vec{\mathcal{P}}_i^{(k)} - \vec{\mathcal{P}}_j^{(l)} + \vec{R} + \delta \vec{e}_n| \tag{A19b}$$

and

$$b_{ij} = |\vec{r}_i - \vec{r}_j + \vec{R}| \ . \tag{A19c}$$

The subscript n stands for x and y, respectively.

3. *Construction of defects*

The procedure we adopt is the following: In a first step we construct an initial configuration which, after relaxation, will contain the desired defect. For vacancies and divacancies, this is easily achieved by removing particles from a perfect triangular system; for interstitials, by adding a particle.

For dislocations, the situation is a bit more complicated. While dislocation pairs in a square lattice can be obtained by removing a number of adjacent particles in a row, in the case of a triangular lattice a 120 degrees "zig zag" of particles has to be removed. After relaxing the system, one obtains dislocation pairs whose (antiparallel) Burger's vectors are at approximately a 90° angle to their separation vector. By adding particles to this system at suitable positions, one can then obtain dislocation pairs with an arbitrary angle between the Burger's and separation vector.

In order to obtain initial configurations which, after relaxation will contain grain boundaries, we take a perfect lattice and apply suitable symmetry operations to the positions of a subset of particles.

In order to relax such a given initial configuration $\{\vec{r}_j^{(0)}\}$, one then moves the particles by distances $\delta\vec{r}_j^{(0)}$ in proportion to the forces $\vec{F}_j^{(0)}$ acting on the particles. This leads to a new configuration $\{\vec{r}_j^{(1)}\}$

$$\vec{r}_j^{(1)} = \vec{r}_j^{(0)} + \alpha \vec{F}_j^{(0)} \ . \tag{A20}$$

This process is repeated until convergence is obtained. In practice, the convergence can be monitored by calculating the energy for subsequent configurations. Clearly, the convergence of this relaxation scheme depends upon the choice of the parameter α in Eq. (A20). This can be seen most easily in the linear regime, where the forces $\vec{F}_j$ can be represented in the form

$$\vec{F}_j = -\sum_k A_{jk}(\vec{r}_j - \vec{r}_j^{\,eq}) \ , \tag{A21}$$

where the equilibrium positions of the particles are denoted by $\vec{r}_j^{\,eq}$ and A_{jk} is the dynamical matrix. In this linear regime, the relaxation equation (A20) takes the form

$$\vec{y}_j^{(i+1)} = \vec{y}_j^{(i)} - \alpha \sum_k A_{jk} \vec{y}_k^{(i)} \ . \tag{A22}$$

where $\vec{y}_j^{(i)} = \vec{r}_j^{(i)} - r_j^{eq}$. Denoting the largest eigen-

TABLE IV: Comparison of numerical and analytic results for the energy per particle of a perfect triangular (E^{Δ}) and square ($E^{\square}$) lattice with various values of the mesh size Δ and the parameter, N_c, the number of particles inside the cutoff radius, R_c, in the numerical computations (see the Appendix).

N_c	Δ/L	$-E^{\Delta}(\epsilon_0)$	$-E^{\square}(\epsilon_0)$	$E^{\square}(\epsilon_0)-E^{\Delta}(\epsilon_0)$
19	1/128	1.950 550	1.937 909	0.012 641
37	1/128	1.953 338	1.942 983	0.010 355
37	1/256	1.958 735	1.948 341	0.010 394
91	1/256	1.959 372	1.949 006	0.010 366
Exact		1.960 516	1.950 132	0.010 384

value of the dynamical matrix by ω^2, we see that the iteration will converge provided that

$$|1-\alpha\omega^2|<1 \quad . \tag{A23}$$

An estimate for the eigenvalue ω^2 can be obtained from its value for the perfect crystal, where ω is given by the frequency of the longitudinal phonon at the zone boundary. The best convergence is obtained by choosing α close below the maximum allowed value

$$\alpha_{\max}=\frac{2}{\omega^2} \quad . \tag{A24}$$

4. *Discussion of numerical errors*

As discussed in Appendix section 2, our mesh method leads to a remainder term of order Δ^2 for each pair of particles separated by a distance larger than R_c. For the force it is determined by the third derivative of the Coulomb interaction at that separation, for the energy by the second derivative. Summation over all particles then leads to an error δE in the total energy E

$$\delta E \sim \Delta^2/R_c \tag{A25}$$

and an error $\delta\vec{F}_i$ in the force $\vec{F}_i$ acting on particle i

$$|\delta\vec{F}_i| \sim \Delta^2/R_c^2 \quad . \tag{A26}$$

It is however important to note that for systems whose lattice is commensurate with the mesh, the mesh method will give exact results if the particles lie on mesh points; however, it will lead to errors of the forms (A25) and (A26) if they lie inside the mesh cells. In this case, the error will thus depend quite strongly on the position of the system relative to the mesh. In order to minimize this position dependence, it is therefore natural to use systems whose lattice is incommensurate with the mesh size Δ. For our calculations we have used a system with 26×30 particles and a mesh with 128^2 for relaxation and 256^2 mesh points for the calculation of energies which satisfies the incommensurability criterion, to the extent possible in a finite system. In order to check the quality of our method, we have performed extensive tests. In Table IV we list one such test in which the cutoff and mesh size dependence of the energies obtained for a square and triangular lattice is shown. For the square lattice a system with 28×28 particles is used, for the triangular one, 26×30 particles. For reference, we also list the exact values $E^{\square}$ and E^{Δ}. This comparison shows that while the energies themselves depend quite strongly on the cutoff R_c and mesh size $\Delta=L/M$, the difference between the energies of the triangular and square lattices is much less sensitive and approaches the exact value closely.

[1]See, e.g., C. C. Grimes, Surf. Sci. 73, 379 (1978) for a review.

[2]C. C. Grimes and G. Adams, Phys. Rev. Lett. 42, 795 (1979).

[3]D. S. Fisher, B. I. Halperin, and P. M. Platzman, Phys. Rev. Lett. 42, 798 (1979).

[4]L. Bonsall and A. A. Maradudin, Phys. Rev. B 15, 1959 (1977).

[5]P. M. Platzman and H. Fukuyama, Phys. Rev. B 10, 3150 (1974).

[6]J. M. Kosterlitz and D. J. Thouless, J. Phys. C 6, 1181 (1973); and Prog. Low Temp. Phys. (to be published); J. M. Kosterlitz, J. Phys. C 7, 1046 (1974).

[7]B. I. Halperin and D. R. Nelson, Phys. Rev. Lett. 41, 121 (1978), 41, 519 (E) (1978); D. R. Nelson and B. I. Halperin, Phys. Rev. B 19, 2457 (1979).

[8]A. P. Young, Phys. Rev. B 19, 1855 (1979).

[9]See, for instance, F. R. N. Nabarro, *Theory of Crystal Dislocations* (Clarendon, Oxford, 1967).

[10]D. J. Thouless, J. Phys. C 11, L189 (1978).

[11]W. T. Read and W. Shockley, Phys. Rev. 78, 275 (1950).
[12]R. W. Hockney and T. R. Brown, J. Phys. C 8, 1813 (1975).
[13]R. Morf, Phys. Rev. Lett. 43, 931 (1979).
[14]R. C. Gann, S. Chakravarty, and G. V. Chester, Phys. Rev. B 20, 326 (1979).
[15]R. E. Peierls, Ann. Inst. Henri Poincaré 5, 177 (1935); L. D. Landau, Phys. Z. Sowjetunion 11, 26 (1937) [*Collected Papers of L. D. Landau,* edited by D. ter Haar (Gordon and Breach, New York, 1965), p. 193]; N. D. Mermin, Phys. Rev. 176, 250 (1968).
[16]This result has been verified analytically by D. S. Fisher (unpublished).
[17]R. W. Hockney, S. P. Goel, and J. W. Eastwood, J. Comp. Phys. 14, 148 (1974).